In the mouse, prostaglandin D2 signalling protects the endometrium against adenomyosis

Pascal Philibert, Stéphanie Déjardin, Nelly Pirot, Alain Pruvost, Anvi Laetitia Nguyen, Florence Bernex, Francis Poulat, Brigitte Boizet-Bonhoure

In the mouse, prostaglandin D2 signalling protects the endometrium against adenomyosis

Running title : Prostaglandin D2 inhibits uterine adenomyosis

Pascal Philibert[1, 2], Stéphanie Déjardin[1], Nelly Pirot[3,4], Alain Pruvost[5], Anvi Laetitia Nguyen[5], Florence Bernex[3,4], Francis Poulat[1] and Brigitte Boizet-Bonhoure[1*]

[1]Institut de Génétique Humaine, Centre National de la Recherche Scientifique, Université de Montpellier, 34396 Montpellier, France [2]Laboratoire de Biochimie et Biologie Moléculaire, Hôpital Carèmeau, CHU de Nîmes, 30029 Nîmes, France [3]Institut de Recherche en Cancérologie de Montpellier IRCM, Université de Montpellier, ICM, INSERM, 34298 Montpellier, France [4]BioCampus, RHEM, Université de Montpellier, CNRS, INSERM,

Montpellier, France [5]Université Paris Saclay, CEA, INRAE, Département Médicaments et Technologies pour la Santé (DMTS), SPI, 91191 Gif-sur-Yvette, France.

***Correspondence address:** Institut de Génétique Humaine, CNRS UMR9002, Université de Montpellier, 141, rue de la Cardonille, 34396 Montpellier Cedex5, France; phone: 33 (4) 34 35 99 40

Abstract

Adenomyosis is characterised by epithelial gland and mesenchymal stroma invasion of the uterine myometrium. Adenomyosis is an oestrogen-dependent gynaecological disease in which a number of factors, such as inflammatory molecules, prostaglandins (PGs), angiogenic factors, cell proliferation and extracellular matrix remodelling proteins also play a role as key disease mediators. In this study, we used mice lacking both L- and H-*prostaglandin D synthase* (*Pgds*) genes in which PGD2 is not produced to elucidate PGD2 roles in the uterus. Gene expression studied by real-time PCR and hormone dosages performed by ELISA or liquid chromatography tandem mass spectroscopy (LC-MS/MS) in mouse uterus samples, showed that components of the PGD2 signalling pathway, both PGDS and PGD2-receptors, are expressed in the mouse endometrium throughout the oestrus cycle with some differences among uterine compartments. We showed that PGE2 production and the steroidogenic pathway are dysregulated in the absence of PGD2. Histological analysis of *L/H-Pgds*$^{-/-}$ uteri, and immunohistochemistry and immunofluorescence analyses of proliferation (Ki67), endothelial cell (CD31), epithelial cell (pan-

cytokeratin), myofibroblast (a-SMA) and mesenchymal cell (vimentin) markers, identify that 6-month-old *L/H-Pgds*$^{-/-}$ animals developed adenomyotic lesions, and that disease severity increased with age. In conclusion, this study suggests that the PGD2 pathway has major roles in the uterus by protecting the endometrium against adenomyosis development. Additional experiments, using for instance transcriptomic approaches, are necessary to fully determine the molecular mechanisms that lead to adenomyosis in *L/H-Pgds*$^{-/-}$ mice and to confirm whether this strain is an appropriate model for studying the human disease.

Key words: adenomyosis, endometrium, prostaglandin D2, mouse model, Prostaglandin E2

Introduction

Adenomyosis is defined as the presence of ectopic endometrial glands and mesenchymal stroma in the uterine myometrium (Benagiano *et al.*, 2014, Bergeron *et al.*, 2006). Conversely, endometriosis is defined as the presence of endometrial tissue (glands and stroma) in organs other than the uterus, such as ovaries, gastrointestinal

tract and peritoneal cavity. Both diseases are characterised by severe pelvic and abdominal pain (Bozdag, 2015) and contribute to fertility disorders and infertility (Campo *et al.* , 2012). Adenomyosis/endometriosis affects 10% of women of reproductive age and is detected in 20 to 50% of women with infertility (Mahmood and Templeton, 1991, Bozdag, 2015). Adenomyosis pathogenesis is multifactorial and different from that of endometriosis (Guo, 2020). It has been linked to abnormal functions of the endometrial-myometrial interface that comprises the junctional zone (JZ) (Leyendecker *et al.*, 2009, Yen *et al.*, 2017, Tanos *et al.*, 2020). The JZ structure derives embryologically from the paramesonephric ducts, while the remaining myometrium has a mesenchymal origin. Importantly, in the nonpregnant uterus peristalsis originates from the JZ through steroid hormone-dependent stimulations (Lyons *et al.*, 1991). Uterine hyperperistalsis is caused by a physiological stress, such as an increased oestrogen production at the endometrial-JZ and might lead to microtrauma, inflammation and repair (Leyendecker *et al.*, 2009). These tissue injury and repair processes may be responsible for the basal endometrium invagination into the JZ layer and adenomyosis development (Garcia-Solares *et al.*, 2018, Vannuccini *et al.*, 2017). However, adenomyosis pathophysiology is still not fully understood.

Murine models with genetic modifications enabling the study of adenomyosis have been identified; for example, constitutive activation of β-catenin (Oh *et al.*, 2013) or FSH receptor haploinsufficiency (Danilovich *et al.* , 2002) in the uterus, promotes adenomyosis development. Moreover, a heterozygous mutation of the *Brca2* gene increases adenomyosis frequency in 6-month-old diethylstilboestrol-treated 129/Sv mice (Bennett *et al.* , 2000). Furthermore, to identify adenomyosis biomarkers and to develop new targeted and individualised treatments, murine models of adenomyosis have been developed (Bruner-Tran *et al.*, 2018, Greaves and White, 2006,Yen *et al.*, 2017). They include progesterone administration (Ostrander *et al.* , 1985), anterior pituitary isografting in the uterine lumen leading to overexposure to prolactin (Mori *et al.* , 1981), short-time exposure to tamoxifen (Green *et al.* , 2005, Mehasseb *et al.* , 2009, Parrott *et al.* , 2001, Shen *et al.* , 2016), and exposure prenatally or after sexual maturity to the synthetic oestrogen ethynyl oestradiol (Koike *et al.* , 2013). Exposure to endocrine-disrupting compounds, such as dioxin (Bruner-Tran *et al.*, 2016), diethylstilboestrol (Ostrander *et al.*, 1985) or bisphenolA (Newbold *et al.*, 2007) also has been associated with adenomyosis occurrence in mice (Bruner-Tran *et al.*, 2017). An

epidemiology study suggested that dioxin exposure might promote adenomyosis development in women (Heilier *et al.*, 2005).

Adenomyosis is an oestrogen-dependent disease, causing chronic inflammation (Kitawaki, 2006), in which a number of factors, such as inflammatory molecules, angiogenic factors, cell proliferation and extracellular matrix remodelling proteins also play a role as key disease mediators (Benagiano *et al.*, 2014). In turn, infiltration of endometrial glands and stroma into the myometrium and hyperestrogenism will activate myometrial peristalsis leading to the activation of the tissue injury and repair mechanism, followed by chronic inflammation (Leyendecker *et al.*, 2009, Guo, 2020). For instance, oestrogen-dependent upregulation of prostaglandin endoperoxide synthase 2 (COX-2) induces excess production of prostaglandin E2 (PGE2) in peritoneal endometriotic lesions (Bulun, 2009, Wu *et al.*, 2007). In turn, PGE2 through its EP2 receptor is a potent inducer of aromatase, specifically in ectopic stromal cells (Bulun, 2009), leading to abnormal oestrogen production. Consequently, the progression and spread of adenomyosis lesions might result from oestrogen-activated epithelial-mesenchymal transition (EMT) through activation of the TGF-β1-Smad3 signalling pathway as observed in a mouse model of adenomyosis (Shen *et al.*, 2016) and in human

adenomyotic tissue samples (Liu *et al.* , 2016). Prostaglandins are implicated in female reproductive tract physiology, including ovulation, implantation, cervical dilation, menstrual cycle, luteolysis, myometrial contractility, placental vascular tone and parturition (Kennedy *et al.*, 2007, Lim and Dey, 1997, Lim and Dey, 2002). They have been involved in endometrial pathologies such as dysmenorrhoea, endometriosis and uterine adenocarcinoma (Sales and Jabbour, 2003). PGE2 and PGF2 synthases are strongly expressed in human (Catalano *et al.*, 2011), rat (Satoh *et al.*, 2013) and mouse endometrium (Liu *et al.*, 2017). Conversely, prostaglandin D2 (PGD2) synthase expression is lower in human endometrium (Catalano *et al.*, 2011), and PGD2 production is 2-3 times lower than that of PGE2 in rat endometrium (Chaud *et al.*, 1994). In the mouse, the major prostanoid involved in myometrial contraction, is PGD2 (Liu *et al.*, 2017) and has been associated with preterm birth (Kumar *et al.*, 2015). In the porcine uterus, PGD2 antagonises PGE2 and PGF2α effects and inhibits contraction of the longitudinal muscle layer (Cao *et al.*, 2005). These data suggest that besides PGE2 and PGF2α, PGD2 also has major role(s) in uterine physiology.

PGD2 is produced from the instable precursor PGH2 by two different PGD2 synthases (PGDS) enzymes, Lipocalin and Hematopoietic-type (L-PGDS and H-

PGDS) encoded by distinct genes (*L-* and *H-PGDS*, official name: *PTGDS/Ptgds* and *HPGDS/Hpgds* in the human and mouse genome, respectively but referred to as *L-Pgds* for *Ptgds* and *H-Pgds* for *Hpgds*, respectively in this manuscript). To elucidate PGD2 roles in the uterus, we analysed the expression of both PGD2 synthases and both PGD2 receptors in the normal mouse uterus and then, characterised the double-knock-out *L/H-Pgds*$^{-/-}$ mouse strain in which PGD2 is not produced due to invalidation of both *L-Pgds* and *H-Pgds* genes (Moniot *et al.*, 2014). We found that in *L/H-Pgds*$^{-/-}$ uteri, steroidogenic and prostaglandins pathways were dysregulated, uterine structures (endometrial stroma, JZ and myometrium) were modified, and that *L/H-Pgds*$^{-/-}$ females developed adenomyosis from the age of 6 months. These data suggest that the PGD2 pathway has major roles in the uterus by protecting the endometrium against adenomyosis development.

Materials and Methods

L/H-Pgds$^{-/-}$ mouse strain maintenance and tissue collection

Animal care and handling followed the Réseau des Animaleries de Montpellier (RAM) guidelines and all procedures were approved by the Regional Ethical Committee (agreement number 34-366 for B.B.-B.). Double-mutant *L/H-Pgds*$^{-/-}$ and wild type (WT) *L/H-Pgds*$^{+/+}$ mice in the 129/Sv genetic background (Mohri *et al.*, 2006, Trivedi *et al.*, 2006) were housed at the IGH/IGF animal care facility in controlled environmental conditions (light/darkness: 12h/12h, 23 °C). Before sacrifice, the oestrus cycle phase of each female was determined by cytological analysis of a vaginal smear after haematoxylin and eosin (HE) staining (Byers *et al.*, 2012). The proestrus/oestrus stage and metestrus stage were referred as proliferative phase and secretory phase, respectively.

Uteri from 6-, 9- and 12-month-old *L/H-Pgds*$^{-/-}$ and wild type (WT) adult animals (n=16-28, n=10-11 and n=5-15 animals per age and genotype, respectively) were dissected. For each animal, one uterine horn was cut in three pieces that were frozen immediately in dry ice and kept at -80 °C until processing (hormone dosages, RT-qPCR, as described below). The second uterine horn was fixed in 4 w/v % paraformaldehyde/PBS for paraffin embedding.

Histology, immunofluorescence and immunohistochemistry

Uterine tissue sections (3 μm; n=2 per animal) were cut from paraffin-embedded tissue blocks and were processed for histological analysis after HE staining using standard protocols. The

presence of histological hallmarks of adenomyosis was investigated under a microscope. Specifically, the severity of the adenomyotic lesions was scored according to the criteria proposed by Bird and colleagues (Bird *et al.*, 1972), as previously described (Shen *et al.*, 2016): Grade 0, normal uterus; Grade 1 (slight adenomyosis), infiltration of endometrial tissue into the surface of the inner myometrium layer; Grade 2 (moderate adenomyosis), invasion of endometrial stroma and glands into the inner myometrium layer; Grade 3 (severe adenomyosis), penetration in the connective tissue between the inner and outer myometrial layers. Uterine adenomyosis frequency in WT and *L/H-Pgds* $^{-/-}$ animals at each age was quantified as the percentage of animals without adenomyosis (Grade 0, and with adenomyosis (Grade 1-3) relative to all analysed animals. Collagen deposition was assessed by staining deparaffinised tissue sections with 0.1% picro-Sirius red solution for 1h, according to the manufacturer's instructions, followed by rinsing with acidified water and air-drying.

Immunohistochemistry (IHC) was performed using a VENTANA Discovery Ultra automated staining instrument (Ventana Medical Systems, Tuscon, AZ, USA), VENTANA reagents, according to the manufacturer's instructions, and the antibodies listed in Supplementary Table SI. Sections were counterstained with haematoxylin for 4 min and dehydrated before coverslip addition. Histology and IHC slides were scanned with a

Nanozoomer Hamamatsu device (Hamamatsu Photonics, Tokyo, Japan) and analysed with the Nanozoomer Digital Pathology (NDPview2) software (Hamamatsu Photonics).

Immunofluorescence (IF) analysis of deparaffinized tissue sections was performed as previously described (Moniot *et al.*, 2009, Rossitto *et al.*, 2019a). Primary and secondary antibodies and their dilutions are listed in Supplementary Table SI. The antibody specificity was confirmed by performing the same IF experiment without primary antibody (not shown). IF images were captured with a Zeiss AxioImager apotome microscope (Carl Zeiss Microscopy, Jena, Germany) or by scanning slides with a Zeiss AxioScan (Carl Zeiss).

Histology, IHC and IF images were processed with the OMERO software (OMERO. web 5.5.1, University of Dundee and Open Microscopy Environment). Ki67 and CD31 immunostaining of mouse uteri was evaluated using a semi-quantitative scoring system. Five regions of interest (ROIs) in the endometrial stroma, JZ and inner myometrium compartments were randomly selected in three sections of six mouse uteri for each marker. Ki67 and CD31-positive cells were segmented using the CellProfiler Software (2.2.0, Broad institute of Harvard, www.cellprofiler.org) (Jones *et al.*, 2008), and the signal intensity was measured. PGDS and CYP19a1 expression levels in mouse uteri (n=3 to 5) were quantified with the OMERO software in ROIs (n=3 to 4) for different uterine compartment. The mean staining

intensity values from IHC and IF experiments were compared between groups with the Graph Prism8 software (San Diego, CA, USA).

RNA extraction and quantitative realtime RT-PCR

RNA was extracted from mouse uterine samples (50-100 mg) using Trizol reagent (Thermo Fisher Scientific, Waltham, MA, USA). For each sample (n=5 for each genotype and for each oestrous cycle phase), two independent reverse transcription (RT) (SuperScriptIV; Thermo Fisher Scientific) reactions were done using 800 ng of total RNA, as previously described (Moniot *et al.*, 2009). Real-time PCR runs (n=3) were performed using each RT product on a LightCycler 480 apparatus (Roche Diagnostics) and the primers listed in Supplementary Table SII. *18S* was used as a reference gene for PCR data normalization. Data were compared with the GraphPrism 8 software (San Diego, CA, USA).

Progesterone, oestradiol and prostaglandin assays

Steroids were extracted (twice) from uterine tissue samples (30 to 70 mg) with diethyl-ether (progesterone or prostaglandins) or methanol (17β-oestradiol). After evaporation, extracts were resuspended in EIA buffer (Cayman Chemical, Ann Arbor, MI, USA). Progesterone was quantified in WT and *L/H-Pgds*$^{-/-}$ uteri (n=4 to 7 for each group) in proliferative and secretory

phases, by liquid chromatography–tandem mass spectrometry (LC-MS/MS) as described in (Rossitto *et al.*, 2019b). Seventeen β-oestradiol was quantified in control (WT) (n=6), and *L/H-Pgds-/-* (n=6) uteri in the proliferative phase using the Oestradiol EIA kit (Cayman Chemical 582251). Prostaglandins (PGD2, PGE2, PGF2α, PGI2) in WT and *L/H-Pgds-/-* uteri (n=4 to 7 for each group) in proliferative and secretory phases, were quantified using the ProstaglandinD2-MOX, ProstaglandinE2-Express, Prostaglandin F2α and Prostaglandin I metabolite EIA Kits (Cayman Chemical 512011, 500141, 516011 and 501100, respectively), according to the manufacturer's instructions. Steroid levels were normalised to the uterine sample weight and expressed in pg/mg tissue.

Statistical analysis

Statistical analyses were performed with GraphPrism 8 software (San Diego, CA, USA). For RT-qPCR and for prostaglandin and steroid concentrations, values are the mean ± SEM of different experiments and of different uterine samples (n=5) for each group. The Student's *t* test was used to compare WT and *L/H-Pgds* $^{-/-}$ groups in independent experiments, and the one-way analysis of variance (ANOVA) with Tukey post hoc pairwise comparison was used when comparing more than two groups. A P-value <0.05 was considered significant (*P<0.05, **P<0.01, ***P<0.005, ****P<0.0001).

Results

Expression of PGD2 synthases in the mouse uterus

We evaluated *L-Pgds* and *H-Pgds* expression by RT-qPCR in 6-month-old WT uteri collected at the proliferative (proestrus/oestrus) and secretory (metestrus) phases. *L-Pgds* expression was comparable (*P>0.05*) between phases and was significantly higher (2.5-fold) than that of *H-Pgds* in the proliferative phase (*P<0.05*) but not in the secretory phase (Figure 1A). Conversely, *H-Pgds* expression was significantly higher in the secretory (2.8-fold) than proliferative phase (*P<0.005*) (Figure 1A). Moreover, in mouse uteri, quantification of the IF staining intensity showed that L-PGDS expression in the inner myometrium layer (iml) and JZ was significantly (*P<0.0001* and *P<0.05*, respectively) higher in the proliferative phase than in the secretory phase. Conversely, L-PGDS expression level in endometrial stroma (ES), and glandular/luminal epithelia (GE/LE) was not significantly different between phases (Figure 1B, C). In the proliferative phase, L-PGDS expression level was significantly higher in the inner iml than in ES (*P<0.01*) and in LE than in ES (*P<0.05*). In the secretory phase, the highest L-PGDS expression levels were in the LE (*P<0.01* and *P<0.05* compared with iml and JZ). H-

PGDS protein expression was not oestrus cycle-dependent but in each phase, expression in the LE was significantly higher than in the other compartments (*P<0.0005*) (Figure 1B, D).

The PGD2 receptors DP1 (Boie *et al.* , 1995) (Figure 1E) and DP2 ((Hirai *et al.* , 2001) (Figure 1F) also were expressed in the different uterine compartments; DP1 expression was similar to H-PGDS expression, and DP2 strongly overlapped with L-PGDS expression. These results show that both PGDS and PGD2-receptors are expressed in the mouse uterus throughout the oestrus cycle with some differences among uterine compartments.

Lack of PGD2 modifies prostaglandin production in *L/H-Pgds*$^{-/-}$ uteri

RT-qPCR quantification showed that uterine expression of the genes encoding the PGI2 (*Pgis*) and PGF2α (*Akr1b3*) synthases was significantly decreased in *L/H-Pgds*$^{-/-}$ mice compared with WT samples in the proliferative phase (*P<0.01* and *P<0.05*, respectively), but not in the secretory phase (Figure 2A and B). Expression of PGE2 synthases (*Pges-1*, *Pges-2* and *cPges*) was not significantly different between WT and *L/H-Pgds*$^{-/-}$ uteri. Conversely, *Cox-1* and *Cox-2* levels were respectively higher and lower in the proliferative phase, and vice versa in the secretory phase in *L/H-Pgds*$^{-/-}$ uteri compared with control uteri (Figure 2A and B). The level of *15-Pgdh* (encoding 15-hydroxyprostaglandin dehydrogenase*,* the major enzyme for prostaglandin degradation), was significantly increased in *L/H-Pgds*$^{-/-}$ uteri (*P=<0.0001*) only in

the secretory phase. IF staining indicated that PGES-1 expression level was increased in ES cells and in the hyperplasic LE of *L/H-Pgds*$^{-/-}$ uteri compared with control (Supplementary Figure S1A). Moreover, COX-1 and COX-2 levels were significantly increased in *L/H-Pgds*$^{-/-}$ ES (cytoplasmic localization) (*P<0.0001* and *P<0.01*, respectively), whereas in LE they did not differ between genotypes (Supplementary Figure S1B-C, Figure 2C).

Consequently, we observed a significant increase of PGE2 level in *L/H-Pgds*$^{-/-}$ uteri in the secretory phase (*P<0.05*) but not in the proliferative phase uteri (*P>0.05*) (Figure 2D). Conversely, PGF2α secretion was not significantly different in WT and *L/H-Pgds*$^{-/-}$ at both phases, although PGF2α level tended to decrease in *L/H-Pgds*$^{-/-}$ proliferative uteri (*P>0.05*) (Figure 2E), in agreement with the decreased mRNA expression of its synthase (*Akr1b3*) (Figure 2A). Also, PGI2 secretion was not modified by *L/H-Pgds* invalidation (Figure 2F). Indeed, the level of PGD2 production was significantly lower in *L/H-Pgds*$^{-/-}$ uteri compared with controls (*P<0.005*) (Figure 2G).

These results suggested that in *L/H-Pgds*$^{-/-}$ mice, the absence of PGD2 production leads to deregulation of PGE2, and to a lesser extent of PGF2α production.

Impaired steroidogenesis in *L/H-Pgds*$^{-/-}$ uteri

As COX-2-induced PGE2 production is oestrogen-dependent (Wu *et al.*, 2007) and in uterine

tissue with endometriosis, 17β-oestradiol (E2) production depends on the local steroid metabolism (Huhtinen *et al.* , 2012a), we compared the expression of genes implicated in steroidogenesis in WT and *L/H-Pgds*$^{-/-}$ mouse uteri. During the proliferative phase, the genes encoding steroidogenic acute regulatory (*StAR) (P=0.0001)*, progesterone receptor (*Pr)* (*P<0.05*) and oestrogen receptors (*Erα* and *Erβ)* (*P<0.005* and *P<0.01*) were significantly upregulated in *L/H-Pgds*$^{-/-}$ uteri compared with controls. Conversely, mRNA expression of the genes encoding cholesterol side-chain cleavage (*Scc),* P450 aromatase (*Cyp19a1)* and vascular endothelial growth factor (*Vegf*) was comparable between genotypes (Figure 3A).

Steroid quantification showed that uterine E2 concentration was not different between genotypes (*P>0.05)*, although it was slightly higher in *L/H-Pgds*$^{-/-}$ uteri (Figure 3B). Conversely, progesterone level was significantly decreased in *L/H-Pgds*$^{-/-}$ uteri, but only in the proliferative phase (*P<0.05* compared with WT) (Figure 3C). However, IF analysis showed a significant upregulation of the P450 aromatase CYP19a1 (the enzyme catalysing E2 production) in LE (*P<0.05*) and ES cells (*P<0.01*) in *L/H-Pgds*$^{-/-}$ uteri in the proliferative phase (Figure 3D and E). The oestrogen receptor ESR1 (ERα) was strongly expressed in the nucleus of endometrial cells (stroma and epithelia) of WT uteri (Supplementary Figure S1D), whereas in *L/H-Pgds*$^{-/-}$ samples, it was mostly localised in the cytoplasm of stromal cells and in the nucleus of epithelial cells (Supplementary Figure S1D). The ESR2 receptor (ERβ) was localised in the

nucleus in proliferative *L/H-Pgds*$^{-/-}$ uteri, but was mainly in the cytoplasm of the different cell types in WT uteri (Supplementary Figure S1E).

Oestrogen availability is regulated by the balance between production and metabolism. Besides CYP19a1 that catalyses E2 synthesis, several 17β-hydroxysteroid dehydrogenases (HSD17Bs) contribute to E2 synthesis or metabolism, thus modifying the level of locally available E2 (Delvoux *et al.* , 2009). We found that *Hsd17b7* was significantly upregulated (*P<0.01*) whereas *Hsd17b2* was significantly downregulated (*P<0.0001*) in *L/H-Pgds*$^{-/-}$ compared with WT uteri (Figure 3F). As HSD17B7 catalyses estrone reduction to E2, and HSD17B2 is involved in E2 inactivation via estrone oxidation, this change may lead to increased E2 level in *L/H-Pgds*$^{-/-}$ uteri. The expression of other *Hsd17bs* (*Hsd17b1*, *12*, *4* and *10*) was not modified in *L/H-Pgds*$^{-/-}$ uteri (Figure 3F). Altogether, these results show that in *L/H-Pgds*$^{-/-}$ uteri, lack of PGD2 profoundly modifies the steroidogenic pathway.

Lack of prostaglandin D2 signalling in *L/H-Pgds*$^{-/-}$ uteri promotes adenomyosis development

Comparison of WT and *L/H-Pgds*$^{-/-}$ females at 6 months of age did not highlight any significant difference in body weight, gross genital tract morphology and fertility. However, histological analysis of 6-month-old WT (n=16) and *L/H-Pgds*$^{-/-}$ (n=28) uteri after HE staining (Figure 4A and

B), showed the presence of focal adenomyosis with endometrium invaginated in the myometrium, in 35% (n=9 from 28) of *L/H-Pgds*$^{-/-}$ samples (Figure 4B and C). In these *L/H-Pgds*$^{-/-}$ uteri, adenomyosis severity ranged from slight (Grade 1; n=6, 21.5% of 28) (Figure 4B1-B1'), moderate (Grade 2; n=2, 7.2%) (Figure 4B2-B2') to severe (Grade 3; n=1, 4%) (Figure 4B3-B3') (Figure 4C). In *L/H-Pgds*$^{+/+}$ WT uteri, the endometrium and myometrium layers were well-demarcated (Figure 4A), and adenomyosis lesions were present only in 18.7% (n=3 of 16) of samples (vs 35% in *L/H-Pgds*$^{-/-}$ uteri) (Figure 4C). As the 129/Sv mouse strain used in this study spontaneously develops adenomyosis at low frequency in adult life (Guttner, 1980), our results show that lack of PGD2 signalling increases its rate in this genetic background.

Adenomyosis frequency strongly increased with age to reach 55% in 9-month-old (n= 6/11) (Figure 4C) and 80% in 12-month-old (n=12/15) *L/H-Pgds*$^{-/-}$ animals, while it remained constant (20%) in 9-month-old (n=2/10) (Figure 4C) and 12-month-old (n=1/5) WT mice (Figure 4C and 4D). Disease severity also increased with age. Indeed, 33% (n=5/15) of 12-month-old *L/H-Pgds*$^{-/-}$ animals presented moderate (Grade 2) (Figure 4E1-E1') and severe (Grade 3) (Figure 4E2-E2') adenomyotic lesions compared with 11% (n=3/9) of 6-month-old *L/H-Pgds*$^{-/-}$ animals (Figure 4C).

We then confirmed the presence of epithelial cells in adenomyotic lesions in 6-month-old *L/H-Pgds*$^{-/-}$ uteri by IHC analysis of cytokeratin expression (an epithelial marker) using a pan-

cytokeratin antibody (Figure 5A). We observed pan-cytokeratin-positive glandular epithelial cells in the iml in *L/H-Pgds*$^{-/-}$ uteri (Figure 5A2) and in focal adenomyotic lesions (Figure 5A3, Adm). IHC with an antibody against the myofibroblast and smooth muscle marker alpha-Smooth Muscle Actin (α–SMA) showed strong α–SMA signal in the outer (oml) and inner (iml) myometrium layers in both WT and *L/H-Pgds*$^{-/-}$ uteri, as expected (Figure 5B1, 5B2), but also in the endometrial stroma (ES) in *L/H-Pgds*$^{-/-}$ uteri (Figure 5B2). Adenomyotic lesions containing pan-cytokeratin-positive glands, were surrounded by cells that strongly expressed α–SMA (Figure 5B3, Adm). Finally, staining with picro-sirius red indicated that in WT uteri, collagen fibres were mainly localised in the myometrium and JZ (Figure 5C1). Conversely, in *L/H-Pgds*$^{-/-}$ uteri, picro-sirius red staining became generalised to the ES (Figure 5C2), particularly in areas surrounding adenomyotic lesions (Figure 5C3, Adm). These results suggest that a fibroblast-to-myofibroblast transdifferentiation (FMT) may occur in the ES of *L/H-Pgds-/-* uteri.

We then investigated cell proliferation by IHC with an anti-Ki67 antibody (proliferation marker) (Figure 6A, 6B). The density of Ki67-positive cells was significantly increased in the ES, JZ and iml of *L/H-Pgds*$^{-/-}$ uteri compared with WT samples (*P=<0.0001*) (Figure 6A1-A2, 6B). Expression of CD31 (Figure 6C-6D), a marker of vascular micro-vessels, was significantly increased in the ES, JZ and myometrium of *L/H-Pgds*$^{-/-}$ uteri (*P<0.0001*) (Figure 6C2, 6D). Moreover, in adenomyotic lesions, epithelial and adjacent stromal cells were actively

proliferating (Figure 6A3, Adm) and were surrounded by a high density of CD31-positive cells (Figure 6C3, Adm), suggesting increased vascularisation in *L/H-Pgds*$^{-/-}$ uteri. Finally, expression of vimentin, a marker of mesenchymal cells and of EMT was increased in the ES (Figure 6E1) and in adenomyotic lesions (Figure 6E3, Adm), but not in the myometrium of *L/H-Pgds*$^{-/-}$ uteri compared with WT samples.

Altogether, these results indicated that *L/H-Pgds*$^{-/-}$ uteri display an adenomyosis phenotype characterised by a strong invasion of the inner layer of the myometrium by endometrial and stromal cells.

Discussion

Adenomyosis is an oestrogen-dependent disease characterised by focal or diffuse presence of endometrial tissue within the uterine myometrium (Bergeron *et al.*, 2006); however, its precise aetiology is unknown. In this study, we found that in *L/H-Pgds*$^{-/-}$ 129/sv mice, in which both PGD2 synthase genes are invalidated, the frequency of focal adenomyosis lesions at the age of 6 months was significantly higher than in WT animals and that disease severity increased with age.

Here, we found that both PGDS, which catalyse PGD2 production, are expressed in the cycling mouse uterus, mainly in epithelial and to a lesser extent in stromal cells. H-PGDS protein expression is not dependent on the oestrous phase whereas *H-Pgds* mRNA is up-regulated in the secretory phase, suggesting a post-transcriptional regulation of *H-Pgds* transcripts. Indeed, H-PGDS has been detected in the female reproductive tract (Urade and Eguchi, 2002, Helliwell *et al.*, 2004). L-PGDS is also strongly expressed in myometrium at the proliferative phase and it is globally 2-fold more expressed at the proliferative than secretory phase. This is in agreement with expression data on human (Catalano *et al.*, 2011, Phillips *et al.*, 2011) and rat uterine samples. Conversely, *L-Pgds* is expressed in the endometrium at all oestrous phases (Kengni *et al.*, 2007). PGD2 has been involved in different processes of female reproduction (Rossitto *et al.*, 2015, Saito *et al.*, 2002), and produced by the uterus, plays central roles in pregnancy maintenance (Helliwell *et al.*, 2004) and in labour initiation and progression both in humans (Shiki *et al.*, 2004) and in rats (Kengni *et al.*, 2007). PGD2 has been implicated in COX-1-mediated labour initiation and parturition, since it induces prepartum myometrial contraction *in vitro* through the PGF2α receptor (FP) (Liu *et al.*, 2017) and *in vivo* in rat endometrium (Hu *et al.*, 2018). In the non-pregnant uterus, normal peristalsis depends on the responsiveness of prostanoid receptors that are heterogeneously distributed in the longitudinal and circular muscles of the myometrium. The DP1 receptor together with EP2 and

prostaglandin I2 receptor, is categorised as a relaxant prostanoid receptor, in contrast to the contractile FP, EP1, EP3 receptors (Hu *et al.*, 2018, Cao *et al.*, 2002). The significant expression of both DP receptors in non-pregnant uteri (Catalano *et al.*, 2011, Hu *et al.*, 2018), particularly in the myometrium (Cao *et al.*, 2002, Myatt and Lye, 2004), is in agreement with our data. DP1 and DP2 receptors are expressed in epithelia and DP2 is strongly expressed in the myometrium suggesting additional roles of PGD2 through its own receptors in normal endometrium and myometrium. PGD2 signalling via binding to both DP receptors may interfere with the action of various prostaglandins and of contractile or inhibitory prostanoid receptors, and might play a major role in non-pregnant uterus. The lack of PGD2 in the *L/H-Pgds*$^{-/-}$ uteri, particularly in the myometrium, might lead to the dysregulation of the normal myometrium peristalsis, causing microtrauma, an initial hallmark of adenomyosis development.

We found that PGD2 signalling influences the secretion of PGE2 and PGF2α, two prostaglandins that are key factors in the regulation of uterine pathophysiology. PGE2 and PGF2α have been implicated in endometriosis development, through activation of local oestrogen production (Wu *et al.*, 2007). Furthermore, PGE2 and PGF2α activate *Cox2* expression in a feedback transcriptional loop (Sales *et al.* , 2008). In the absence of PGD2 production, the decreased secretion of PGF2α might be in part a response to the decreased *Cox2* expression in the proliferative *L/H-Pgds*$^{-/-}$ uterus, whereas its up-regulation in the secretory *L/H-Pgds*$^{-/-}$ uterus might be

consecutive to the increased PGE2 secretion. These prostaglandin levels result from the balance between their synthesis and their degradation. All these steps are highly regulated, starting with phospholipase A2 activity that releases arachidonic acid from the cell membrane, and followed by the regulation of COX activities and prostaglandin synthase expression and activities (Seo and Oh, 2017). Their degradation is initiated by their transport via prostaglandin transporter (PGT), and then by 15-PGDH, the main prostaglandin catabolizing enzyme that biologically inactivates prostaglandins and related eicosanoids (Tai *et al.* , 2002). Discrepancies between *15-Pgdh* and *Cox* expression and PGE2/PGF2α secretion might be due to the prostaglandin synthesis compensation that depends on the availability of the PG precursor PGH2 (Korbecki *et al.* , 2014). They might also reflect their variation in the different uterine compartments in which differences would not be visible by analyses (RT-qPCR) performed on whole uteri.

In the absence of PGD2, the proliferative activity of stromal, JZ and myometrial cells was increased, highlighting an anti-proliferative action of PGD2. On the other hand, PGE2 induces, through its receptors EP2 and EP4, proliferation of human endometrial epithelial cells (Jabbour and Boddy, 2003), endometriotic cells (Makabe *et al.*, 2020) and in the rat uteri (Kengni *et al.*, 2007, Kothapalli *et al.*, 2003). This is a new example of antagonism between prostaglandins, as previously reported for blood pressure, sleep, labour and inflammatory responses (Helliwell *et al.*, 2004). This antagonism between PGD2 and PGE2 might represent a key feature in the appearance of adenomyosis lesions in *L/H-Pgds*$^{-/-}$ uteri.

In endometriosis, a positive feedback cycle between oestrogen production and inflammation is observed via overexpression of steroidogenic genes such as *StAR* and *Cyp19a1*, overexpression of COX2 and PGES1, and local secretion of PGE2 and oestradiol (Huhtinen *et al.*, 2012b, Korbecki *et al.*, 2014, Ricciotti and FitzGerald, 2011). PGE2 production in the endometrial stroma enhances transcription of steroidogenic genes necessary for oestrogen synthesis via cAMP-PKA mediated-EP2 receptor signalling (Attar and Bulun, 2006, Attar *et al.* , 2009). The increased PGE2 production in *L/H-Pgds*$^{-/-}$ uteri might be linked to the up-regulation of *StAR* that encodes the rate-limiting factor in steroid biosynthesis; however, *Scc* and *Cyp19a1* transcriptional levels were not changed. CYP19a1 upregulation in *L/H-Pgds*$^{-/-}$ uteri, without any transcriptional modification of the gene expression via PGE2 (Attar *et al.*, 2009), suggests that PGD2 might be involved in CYP19a1 post-transcriptional/translational regulation or in the regulation of its stability (Ghosh *et al.*, 2019, Molehin *et al.*, 2018). Together with CYP19a1 upregulation, the modified expression of HSD17B2 and HSD17B7, two E2 metabolic enzymes, suggests that the local oestrogen metabolism is modified in the absence of PGD2, as reported in human endometriosis (Attar *et al.*, 2009, Delvoux *et al.*, 2009, Huhtinen *et al.*, 2012b) and adenomyosis (Kitawaki, 2006, Maia *et al.*, 2006, Takahashi *et al.*, 1989). Furthermore, in *L/H-Pgds*$^{-/-}$ uteri, the increase in *Esr1* and *Esr2* gene expression followed by the increased nuclear localisation of ESR2 might lead to enhanced estrogenic

response even in the absence of an E2 increase. The differential subcellular localisation of ESR1 and ESR2 is associated with disturbed endometrium and adenomyosis development (Mehasseb *et al.* , 2011) and is observed in mouse models of adenomyotic uterus (Parrott *et al.*, 2001, Bruner-Tran *et al.*, 2017). However, although steroidogenesis was enhanced in the absence of PGD2, 17β–oestradiol production was not significantly increased in *L/H-Pgds*$^{-/-}$ uteri, possibly due to different activities of HSD17B7-mediated E2 synthesis and HSD17B2-mediated E2 catabolism (Huhtinen *et al.*, 2012b). Conversely, progesterone level was significantly decreased in *L/H-Pgds*$^{-/-}$ uteri compared with WT controls. This might be related to the decreased HSD17B2 expression as reported in endometriosis (Dassen *et al.* , 2007). Additional experiments (i.e. high-throughput transcriptomic analysis, *in vitro* analysis) are needed to evaluate the direct or indirect mechanisms initiated by PGD2 and involved in the post-transcriptional/translational regulation of ESR1-2, COX1, COX2, CYP19a1 (Otto *et al.*, 1993, Wada *et al.*, 2009, Yu and Kim, 2012, Jaen *et al.*, 2018, Molehin *et al.*, 2018, Ghosh *et al.*, 2019), thus affecting their expression, stability and/or their subcellular localisation.

Altogether, our study highlights the role of PGD2 in the mouse uterus pathophysiology, showing that two major pathways (i.e. steroidogenesis and prostaglandins) involved in uterine homeostasis are modified in the absence of PGD2 signalling. In *L/H-Pgds*$^{-/-}$ uteri, besides the

alteration of steroidogenesis and its transduction pathways, the modified expression of COX-1, COX-2, PGES-1, CYP19a1, ERα, ERβ in stromal cells and the upregulation of PGE2 production (Figure 7) lead to increased expression of vimentin, suggesting EMT that might enhance epithelial cells invasiveness (Yen *et al.*, 2017). These features could promote cell proliferation and angiogenesis that in turn, might favour tissue inflammation, injury and hyperperistalsis at the JZ and myometrium (Figure 7). The increased expression of α–SMA and collagen I in the *L/H-Pgds*$^{-/-}$ endometrial stroma also suggests myofibroblast differentiation through FMT (Figure 7). These results are also consistent with the presence of α–SMA and collagen I-expressing myofibroblasts and of smooth muscle metaplasia at the endometrium-myometrial JZ leading to adenomyosis development in humans (Ibrahim *et al.* , 2017), and with adenomyosis and endometrial fibrosis induced by tamoxifen or oestrogen-disruptors in mouse models (Parrott *et al.*, 2001, Green *et al.*, 2005, Mehasseb *et al.*, 2009, Ostrander *et al.*, 1985). In the absence of PGD2, myometrial cells proliferation is increased. Consequently, the altered *L/H-Pgds*$^{-/-}$ myometrium and the disorganised fascicles of smooth muscle, with the lack of a membrane layer between stroma and inner myometrium, might facilitate invasion by the overlying stroma (Naftalin and Jurkovic, 2009, Mehasseb *et al.* , 2010, Ibrahim *et al.*, 2017). Abnormal myometrium development has been also reported in tamoxifen-induced adenomyosis (Bruner-Tran *et al.*, 2016). Lack of PGD2 signalling might contribute to the disruption of the inner

myometrial architecture and function, supporting the hypothesis that adenomyosis is primarily the result of a microtrauma at the junction between endometrium and myometrium (Leyendecker *et al.*, 2009). Secondarily, it predisposes the endometrial stroma and glands to infiltration into the myometrium, two events that occur sequentially in adenomyosis development (Brosens *et al.* , 1995).

This *L/H-Pgds*$^{-/-}$ mouse model allowed showing that lack of PGD2 signalling plays an important role in adenomyosis pathogenesis. Additional experiments, using for instance transcriptomic approaches, are necessary to fully determine the molecular mechanisms that lead to adenomyosis in *L/H-Pgds*$^{-/-}$ mice and to confirm whether this strain is an appropriate model for studying adenomyosis. This *L/H-Pgds-/-* mouse model is one of the first genetic models that can be used to investigate *in vivo* the molecular and cellular modifications occurring during adenomyosis development and to test adenomyosis treatments. It would be interesting to determine whether a given treatment may revert the observed phenotype. Moreover, as L-PGDS is the major PGD2 synthase in the mouse uterus, experiments with single *L-* or *H-Pgds* mutants are required.

Acknowledgments

We thank the technical staff (Morgane Broyon, Aurélie Covinhes, Yoan Buscail, Alicia Seguin and Jean Noël) of the “Réseau d’Histologie Expérimentale de Montpellier” - RHEM facility supported by SIRIC Montpellier Cancer (Grant INCa_Inserm_DGOS_12553), the european regional development foundation and the occitanian region (FEDER-FSE 2014-2020 Languedoc Roussillon) for processing our animal tissues, histology analysis and expertise. We are grateful to Dr Marie-Pierre Blanchard and Amélie Sarrazin from the IGH Imaging facility (MRI Montpellier) for their help with microscopy analyses. We thank the staff (particularly Quentin Durix, Luc Forichon, Steeve Thirard, Elodie Belan, Karim Mesbah) of the IGH/IGF animal care facility (Réseau des Animaleries de Montpellier, RAM).

Authors’ roles

P. P. designed the study, performed experiments, data analysis and interpretation. S. D. carried out and analysed RT-qPCR, immunofluorescence analysis on mouse uteri, and hormonal dosages. N. P. designed, performed and interpretated histological data and IHC on mouse samples. A. P. designed and interpretated the LC MS/MS experiments. A.-L. N. performed the LC MS/MS experiments. F. B. analysed and interpretated histological data and

IHC on mouse samples. F. P. interpretated data. B. B.-B. conceived and designed the study, performed data analysis and interpretation. First draft was prepared by B. B.-B. and all authors read the manuscript, revised it and participated in the final version.

Funding

CNRS and University of Montpellier; National Agency for the Safety of Health Products (ANSM), (Grant 2013-041 to B. B.-B.).

Conflict of Interest

None of the authors declared a conflict of interest of any kind.

Data Availability Statement

The data underlying this article are available in the article and in its online supplementary material.The data underlying this article will be shared on reasonable request to the corresponding author.

References

535 Attar E, Bulun SE. Aromatase and other steroidogenic genes in endometriosis: translational
536 aspects. *Hum Reprod Update* 2006;**12**:49-56.

537 Attar E, Tokunaga H, Imir G, Yilmaz MB, Redwine D, Putman M, Gurates B, Attar R,
538 Yaegashi N, Hales DB *et al.* Prostaglandin E2 via steroidogenic factor-1 coordinately regulates
539 transcription of steroidogenic genes necessary for estrogen synthesis in endometriosis. *J Clin*
Endocrinol Metab 2009;**94**:623-631.

541 Benagiano G, Brosens I, Habiba M. Structural and molecular features of the endomyometrium
542 in endometriosis and adenomyosis. *Hum Reprod Update* 2014;**20**:386-402.

543 Bennett LM, McAllister KA, Malphurs J, Ward T, Collins NK, Seely JC, Gowen LC, Koller
544 BH, Davis BJ, Wiseman RW. Mice heterozygous for a Brca1 or Brca2 mutation display distinct
545 mammary gland and ovarian phenotypes in response to diethylstilbestrol. *Cancer Res*
546 2000;**60**:3461-3469.

547 Bergeron C, Amant F, Ferenczy A. Pathology and physiopathology of adenomyosis. *Best Pract*
Res Clin Obstet Gynaecol 2006;**20**:511-521.

549 Bird CC, McElin TW, Manalo-Estrella P. The elusive adenomyosis of the uterus--revisited. *Am*
J Obstet Gynecol 1972;**112**:583-593.

551 Boie Y, Sawyer N, Slipetz DM, Metters KM, Abramovitz M. Molecular cloning and
552 characterization of the human prostanoid DP receptor. *J Biol Chem* 1995;**270**:18910-18916.

553 Bozdag G. Recurrence of endometriosis: risk factors, mechanisms and biomarkers. *Womens*
Health (Lond) 2015;**11**:693-699.

555 Brosens JJ, de Souza NM, Barker FG. Uterine junctional zone: function and disease. *Lancet*
556 1995;**346**:558-560.

557 Bruner-Tran KL, Duleba AJ, Taylor HS, Osteen KG. Developmental Toxicant Exposure Is
558 Associated with Transgenerational Adenomyosis in a Murine Model. *Biol Reprod* 2016;**95**:73.
559 Bruner-Tran KL, Gnecco J, Ding T, Glore DR, Pensabene V, Osteen KG. Exposure to the
560 environmental endocrine disruptor TCDD and human reproductive dysfunction: Translating
561 lessons from murine models. *Reprod Toxicol* 2017;**68**:59-71.
562 Bruner-Tran KL, Mokshagundam S, Herington JL, Ding T, Osteen KG. Rodent Models of
563 Experimental Endometriosis: Identifying Mechanisms of Disease and Therapeutic Targets.
Curr Womens Health Rev 2018;**14**:173-188.
565 Bulun SE. Endometriosis. *N Engl J Med* 2009;**360**:268-279.
566 Byers SL, Wiles MV, Dunn SL, Taft RA. Mouse estrous cycle identification tool and images.
PLoS One 2012;**7**:e35538.
568 Campo S, Campo V, Benagiano G. Adenomyosis and infertility. *Reprod Biomed Online*
569 2012;**24**:35-46.
570 Cao J, Shayibuzhati M, Tajima T, Kitazawa T, Taneike T. In vitro pharmacological
571 characterization of the prostanoid receptor population in the non-pregnant porcine myometrium.
Eur J Pharmacol 2002;**442**:115-123.
573 Cao J, Yosida M, Kitazawa T, Taneike T. Uterine region-dependent differences in
574 responsiveness to prostaglandins in the non-pregnant porcine myometrium. *Prostaglandins
Other Lipid Mediat* 2005;**75**:105-122.
576 Catalano RD, Wilson MR, Boddy SC, Jabbour HN. Comprehensive expression analysis of
577 prostanoid enzymes and receptors in the human endometrium across the menstrual cycle. *Mol
Hum Reprod* 2011;**17**:182-192.
579 Chaud M, Faletti A, Beron de Estrada M, Gimeno AL, Gimeno MA. Synthesis and release of
580 prostaglandins D2 and E2 by rat uterine tissue throughout the sex cycle. Effects of 17-beta-
581 estradiol and progesterone. *Prostaglandins Leukot Essent Fatty Acids* 1994;**51**:47-50.

582 Danilovich N, Roy I, Sairam MR. Emergence of uterine pathology during accelerated biological
583 aging in FSH receptor-haploinsufficient mice. *Endocrinology* 2002;**143**:3618-3627.
584 Dassen H, Punyadeera C, Kamps R, Delvoux B, Van Langendonckt A, Donnez J, Husen B,
585 Thole H, Dunselman G, Groothuis P. Estrogen metabolizing enzymes in endometrium and
586 endometriosis. *Hum Reprod* 2007;**22**:3148-3158.
587 Delvoux B, Groothuis P, D'Hooghe T, Kyama C, Dunselman G, Romano A. Increased
588 production of 17beta-estradiol in endometriosis lesions is the result of impaired metabolism. *J
Clin Endocrinol Metab* 2009;**94**:876-883.
590 Garcia-Solares J, Donnez J, Donnez O, Dolmans MM. Pathogenesis of uterine adenomyosis:
591 invagination or metaplasia? *Fertil Steril* 2018;**109**:371-379.
592 Ghosh D, Egbuta C, Kanyo JE, Lam TT. Phosphorylation of human placental aromatase
593 CYP19A1. *Biochem J* 2019;**476**:3313-3331.
594 Greaves P, White IN. Experimental adenomyosis. *Best Pract Res Clin Obstet Gynaecol*
595 2006;**20**:503-510.
596 Green AR, Styles JA, Parrott EL, Gray D, Edwards RE, Smith AG, Gant TW, Greaves P, Al-
597 Azzawi F, White IN. Neonatal tamoxifen treatment of mice leads to adenomyosis but not
598 uterine cancer. *Exp Toxicol Pathol* 2005;**56**:255-263.
599 Guo SW. The Pathogenesis of Adenomyosis vis-a-vis Endometriosis. *J Clin Med* 2020;**9**.
600 Guttner J. Adenomyosis in mice. *Z Versuchstierkd* 1980;**22**:249-251.
601 Heilier JF, Nackers F, Verougstraete V, Tonglet R, Lison D, Donnez J. Increased dioxin-like
602 compounds in the serum of women with peritoneal endometriosis and deep endometriotic
603 (adenomyotic) nodules. *Fertil Steril* 2005;**84**:305-312.
604 Helliwell RJ, Adams LF, Mitchell MD. Prostaglandin synthases: recent developments and a
605 novel hypothesis. *Prostaglandins Leukot Essent Fatty Acids* 2004;**70**:101-113.

606 Hirai H, Tanaka K, Yoshie O, Ogawa K, Kenmotsu K, Takamori Y, Ichimasa M, Sugamura K,
607 Nakamura M, Takano S *et al.* Prostaglandin D2 selectively induces chemotaxis in T helper type
608 2 cells, eosinophils, and basophils via seven-transmembrane receptor CRTH2. *J Exp Med*
609 2001;**193**:255-261.
610 Hu C, Liu B, Li H, Wu X, Guo T, Luo W, Zhou Y. Prostaglandin D2 evokes potent uterine
611 contraction via the F prostanoid receptor in postpartum rats. *Eur J Pharmacol* 2018;**836**:11-17.
612 Huhtinen K, Desai R, Stahle M, Salminen A, Handelsman DJ, Perheentupa A, Poutanen M.
613 Endometrial and endometriotic concentrations of estrone and estradiol are determined by local
614 metabolism rather than circulating levels. *J Clin Endocrinol Metab* 2012a;**97**:4228-4235.
615 Huhtinen K, Stahle M, Perheentupa A, Poutanen M. Estrogen biosynthesis and signaling in
616 endometriosis. *Mol Cell Endocrinol* 2012b;**358**:146-154.
617 Ibrahim MG, Sillem M, Plendl J, Chiantera V, Sehouli J, Mechsner S. Myofibroblasts Are
618 Evidence of Chronic Tissue Microtrauma at the Endometrial-Myometrial Junctional Zone in
619 Uteri With Adenomyosis. *Reprod Sci* 2017;**24**:1410-1418.
620 Jabbour HN, Boddy SC. Prostaglandin E2 induces proliferation of glandular epithelial cells of
621 the human endometrium via extracellular regulated kinase 1/2-mediated pathway. *J Clin*
Endocrinol Metab 2003;**88**:4481-4487.
623 Jaen RI, Prieto P, Casado M, Martin-Sanz P, Bosca L. Post-translational modifications of
624 prostaglandin-endoperoxide synthase 2 in colorectal cancer: An update. *World J Gastroenterol*
625 2018;**24**:5454-5461.
626 Kengni JH, St-Louis I, Parent S, Leblanc V, Shooner C, Asselin E. Regulation of prostaglandin
627 D synthase and prostacyclin synthase in the endometrium of cyclic, pregnant, and
628 pseudopregnant rats and their regulation by sex steroids. *J Endocrinol* 2007;**195**:301-311.
629 Kennedy TG, Gillio-Meina C, Phang SH. Prostaglandins and the initiation of blastocyst
630 implantation and decidualization. *Reproduction* 2007;**134**:635-643.

631 Kitawaki J. Adenomyosis: the pathophysiology of an oestrogen-dependent disease. *Best Pract Res Clin Obstet Gynaecol* 2006;**20**:493-502.

633 Koike E, Yasuda Y, Shiota M, Shimaoka M, Tsuritani M, Konishi H, Yamasaki H, Okumoto 634 K, Hoshiai H. Exposure to ethinyl estradiol prenatally and/or after sexual maturity induces 635 endometriotic and precancerous lesions in uteri and ovaries of mice. *Congenit Anom (Kyoto)* 636 2013;**53**:9-17.

637 Korbecki J, Baranowska-Bosiacka I, Gutowska I, Chlubek D. Cyclooxygenase pathways. *Acta Biochim Pol* 2014;**61**:639-649.

639 Kothapalli D, Stewart SA, Smyth EM, Azonobi I, Pure E, Assoian RK. Prostacylin receptor 640 activation inhibits proliferation of aortic smooth muscle cells by regulating cAMP response 641 element-binding protein- and pocket protein-dependent cyclin a gene expression. *Mol Pharmacol* 2003;**64**:249-258.

643 Kumar S, Palaia T, Hall CE, Ragolia L. Role of Lipocalin-type prostaglandin D2 synthase (L-644 PGDS) and its metabolite, prostaglandin D2, in preterm birth. *Prostaglandins Other Lipid Mediat* 2015;**118-119**:28-33.

646 Leyendecker G, Wildt L, Mall G. The pathophysiology of endometriosis and adenomyosis: 647 tissue injury and repair. *Arch Gynecol Obstet* 2009;**280**:529-538.

648 Lim H, Dey SK. Prostaglandin E2 receptor subtype EP2 gene expression in the mouse uterus 649 coincides with differentiation of the luminal epithelium for implantation. *Endocrinology* 650 1997;**138**:4599-4606.

651 Lim H, Dey SK. A novel pathway of prostacyclin signaling-hanging out with nuclear receptors. *Endocrinology* 2002;**143**:3207-3210.

653 Liu B, Yang J, Luo W, Zhang Y, Li J, Li H, Chen L, Zhou Y. Prostaglandin D2 is the major 654 cyclooxygenase-1-derived product in prepartum mouse uteri where it mediates an enhanced in 655 vitro myometrial contraction. *Eur J Pharmacol* 2017;**813**:140-146.

Liu X, Shen M, Qi Q, Zhang H, Guo SW. Corroborating evidence for platelet-induced epithelial-mesenchymal transition and fibroblast-to-myofibroblast transdifferentiation in the development of adenomyosis. *Hum Reprod* 2016;**31**:734-749.

Lyons EA, Taylor PJ, Zheng XH, Ballard G, Levi CS, Kredentser JV. Characterization of subendometrial myometrial contractions throughout the menstrual cycle in normal fertile women. *Fertil Steril* 1991;**55**:771-774.

Mahmood TA, Templeton A. Prevalence and genesis of endometriosis. *Hum Reprod* 1991;**6**:544-549.

Maia H, Jr., Casoy J, Correia T, Freitas L, Pimentel K, Athayde C, Coutinho E. Effect of the menstrual cycle and oral contraceptives on aromatase and cyclooxygenase-2 expression in adenomyosis. *Gynecol Endocrinol* 2006;**22**:547-551.

Makabe T, Koga K, Nagabukuro H, Asada M, Satake E, Taguchi A, Takeuchi A, Miyashita M, Harada M, Hirata T *et al.* Use of selective PGE2 receptor antagonists on human endometriotic stromal cells and peritoneal macrophages. *Mol Hum Reprod* 2020.

Mehasseb MK, Bell SC, Habiba MA. The effects of tamoxifen and estradiol on myometrial differentiation and organization during early uterine development in the CD1 mouse. *Reproduction* 2009;**138**:341-350.

Mehasseb MK, Bell SC, Pringle JH, Habiba MA. Uterine adenomyosis is associated with ultrastructural features of altered contractility in the inner myometrium. *Fertil Steril* 2010;**93**:2130-2136.

Mehasseb MK, Panchal R, Taylor AH, Brown L, Bell SC, Habiba M. Estrogen and progesterone receptor isoform distribution through the menstrual cycle in uteri with and without adenomyosis. *Fertil Steril* 2011;**95**:2228-2235, 2235 e2221.

679 Mohri I, Taniike M, Okazaki I, Kagitani-Shimono K, Aritake K, Kanekiyo T, Yagi T, Takikita
680 S, Kim HS, Urade Y *et al.* Lipocalin-type prostaglandin D synthase is up-regulated in
681 oligodendrocytes in lysosomal storage diseases and binds gangliosides. *J Neurochem* 2006.
682 Molehin D, Castro-Piedras I, Sharma M, Sennoune SR, Arena D, Manna PR, Pruitt K.
683 Aromatase Acetylation Patterns and Altered Activity in Response to Sirtuin Inhibition. *Mol
Cancer Res* 2018;**16**:1530-1542.
685 Moniot B, Declosmenil F, Barrionuevo F, Scherer G, Aritake K, Malki S, Marzi L, Cohen-
686 Solal A, Georg I, Klattig J *et al.* The PGD2 pathway, independently of FGF9, amplifies SOX9
687 activity in Sertoli cells during male sexual differentiation. *Development* 2009;**136**:1813-1821.
688 Moniot B, Ujjan S, Champagne J, Hirai H, Aritake K, Nagata K, Dubois E, Nidelet S,
689 Nakamura M, Urade Y *et al.* Prostaglandin D2 acts through the Dp2 receptor to influence male
690 germ cell differentiation in the foetal mouse testis. *Development* 2014;**141**:3561-3571.
691 Mori T, Nagasawa H, Takahashi S. The induction of adenomyosis in mice by intrauterine
692 pituitary isografts. *Life Sci* 1981;**29**:1277-1282.
693 Myatt L, Lye SJ. Expression, localization and function of prostaglandin receptors in
694 myometrium. *Prostaglandins Leukot Essent Fatty Acids* 2004;**70**:137-148.
695 Naftalin J, Jurkovic D. The endometrial-myometrial junction: a fresh look at a busy crossing.
Ultrasound Obstet Gynecol 2009;**34**:1-11.
697 Newbold RR, Jefferson WN, Padilla-Banks E. Long-term adverse effects of neonatal exposure
698 to bisphenol A on the murine female reproductive tract. *Reprod Toxicol* 2007;**24**:253-258.
699 Oh SJ, Shin JH, Kim TH, Lee HS, Yoo JY, Ahn JY, Broaddus RR, Taketo MM, Lydon JP,
700 Leach RE *et al.* beta-Catenin activation contributes to the pathogenesis of adenomyosis through
701 epithelial-mesenchymal transition. *J Pathol* 2013;**231**:210-222.

Ostrander PL, Mills KT, Bern HA. Long-term responses of the mouse uterus to neonatal diethylstilbestrol treatment and to later sex hormone exposure. *J Natl Cancer Inst* 1985;**74**:121-135.

Otto JC, DeWitt DL, Smith WL. N-glycosylation of prostaglandin endoperoxide synthases-1 and -2 and their orientations in the endoplasmic reticulum. *J Biol Chem* 1993;**268**:18234-18242.

Parrott E, Butterworth M, Green A, White IN, Greaves P. Adenomyosis--a result of disordered stromal differentiation. *Am J Pathol* 2001;**159**:623-630.

Phillips RJ, Al-Zamil H, Hunt LP, Fortier MA, Lopez Bernal A. Genes for prostaglandin synthesis, transport and inactivation are differentially expressed in human uterine tissues, and the prostaglandin F synthase AKR1B1 is induced in myometrial cells by inflammatory cytokines. *Mol Hum Reprod* 2011;**17**:1-13.

Ricciotti E, FitzGerald GA. Prostaglandins and inflammation. *Arterioscler Thromb Vasc Biol* 2011;**31**:986-1000.

Rossitto M, Marchive C, Pruvost A, Sellem E, Ghettas A, Badiou S, Sutra T, Poulat F, Philibert P, Boizet-Bonhoure B. Intergenerational effects on mouse sperm quality after in utero exposure to acetaminophen and ibuprofen. *FASEB J* 2019a;**33**:339-357.

Rossitto M, Ollivier M, Dejardin S, Pruvost A, Brun C, Marchive C, Nguyen AL, Ghettas A, Keime C, de Massy B *et al.* In utero exposure to acetaminophen and ibuprofen leads to intergenerational accelerated reproductive aging in female mice. *Commun Biol* 2019b;**2**:310.

Rossitto M, Ujjan S, Poulat F, Boizet-Bonhoure B. Multiple roles of the prostaglandin D2 signaling pathway in reproduction. *Reproduction* 2015;**149**:R49-58.

Saito S, Tsuda H, Michimata T. Prostaglandin D2 and reproduction. *Am J Reprod Immunol* 2002;**47**:295-302.

725 Sales KJ, Grant V, Jabbour HN. Prostaglandin E2 and F2alpha activate the FP receptor and up-
726 regulate cyclooxygenase-2 expression via the cyclic AMP response element. *Mol Cell Endocrinol* 2008;**285**:51-61.
728 Sales KJ, Jabbour HN. Cyclooxygenase enzymes and prostaglandins in reproductive tract
729 physiology and pathology. *Prostaglandins Other Lipid Mediat* 2003;**71**:97-117.
730 Satoh H, Watanabe K, Kawaminami M, Kurusu S. A comprehensive immunohistochemistry of
731 prostaglandins F2alpha and E2 synthetic enzymes in rat ovary and uterus around parturition. *Prostaglandins Other Lipid Mediat* 2013;**106**:23-28.
733 Seo MJ, Oh DK. Prostaglandin synthases: Molecular characterization and involvement in
734 prostaglandin biosynthesis. *Prog Lipid Res* 2017;**66**:50-68.
735 Shen M, Liu X, Zhang H, Guo SW. Transforming growth factor beta1 signaling coincides with
736 epithelial-mesenchymal transition and fibroblast-to-myofibroblast transdifferentiation in the
737 development of adenomyosis in mice. *Hum Reprod* 2016;**31**:355-369.
738 Shiki Y, Shimoya K, Tokugawa Y, Kimura T, Koyama M, Azuma C, Murata Y, Eguchi N, Oda
739 H, Urade Y. Changes of lipocalin-type prostaglandin D synthase level during pregnancy. *J Obstet Gynaecol Res* 2004;**30**:65-70.
741 Tai HH, Ensor CM, Tong M, Zhou H, Yan F. Prostaglandin catabolizing enzymes. *Prostaglandins Other Lipid Mediat* 2002;**68-69**:483-493.
743 Takahashi K, Nagata H, Kitao M. Clinical usefulness of determination of estradiol level in the
744 menstrual blood for patients with endometriosis. *Nihon Sanka Fujinka Gakkai zasshi*
745 1989;**41**:1849-1850.
746 Tanos V, Lingwood L, Balami S. Junctional Zone Endometrium Morphological Characteristics
747 and Functionality: Review of the Literature. *Gynecol Obstet Invest* 2020;**85**:107-117.

748 Trivedi SG, Newson J, Rajakariar R, Jacques TS, Hannon R, Kanaoka Y, Eguchi N, Colville-
749 Nash P, Gilroy DW. Essential role for hematopoietic prostaglandin D2 synthase in the control
750 of delayed type hypersensitivity. *Proc Natl Acad Sci U S A* 2006;**103**:5179-5184.
751 Urade Y, Eguchi N. Lipocalin-type and hematopoietic prostaglandin D synthases as a novel
752 example of functional convergence. *Prostaglandins & other lipid mediators* 2002;**68-69**:375-
753 382.
754 Vannuccini S, Tosti C, Carmona F, Huang SJ, Chapron C, Guo SW, Petraglia F. Pathogenesis
755 of adenomyosis: an update on molecular mechanisms. *Reprod Biomed Online* 2017;**35**:592-601.
756 Wada M, Saunders TL, Morrow J, Milne GL, Walker KP, Dey SK, Brock TG, Opp MR,
757 Aronoff DM, Smith WL. Two pathways for cyclooxygenase-2 protein degradation in vivo. *J*
Biol Chem 2009;**284**:30742-30753.
759 Wu MH, Shoji Y, Chuang PC, Tsai SJ. Endometriosis: disease pathophysiology and the role of
760 prostaglandins. *Expert Rev Mol Med* 2007;**9**:1-20.
761 Yen CF, Huang SJ, Lee CL, Wang HS, Liao SK. Molecular Characteristics of the Endometrium
762 in Uterine Adenomyosis and Its Biochemical Microenvironment. *Reprod Sci* 2017;**24**:1346-
763 1361.
764 Yu SM, Kim SJ. Protein phosphorylation on tyrosine restores expression and glycosylation of
765 cyclooxygenase-2 by 2-deoxy-D-glucose-caused endoplasmic reticulum stress in rabbit
766 articular chondrocyte. *BMB Rep* 2012;**45**:317-322.

LEGENDS to Figures

Figure 1 Expression of prostaglandin D2 synthases in wild type mouse uterus. (**A**) *L-Pgds* and *H-Pgds* gene expression were analysed by real time quantitative RT-PCR in mouse uteri collected at proliferative (P) and secretory (S) phases of the oestrous cycle. Results were normalised to *18S* mRNA level and were compared with the Student's *t* test; *P<0.05, ***P<0.005. **(B)** Quantification of L-PGDS and H-PGDS staining intensity in the inner myometrium layer (iml), junctional zone (JZ), endometrial stroma (ES), glandular epithelium (GE) and luminal epithelium (LE) (n=3 to 4 regions of interest for each compartment) of proliferative and secretory mouse uterus samples. Staining intensities are the mean +/- SEMs for n=3-5 uterine samples/phase. P-values: *P<0.05, **P<0.01, ***P<0.005, ****P<0.0001. (**C-D**) Representative immunofluorescence panels of L-PGDS (C) and H-PGDS (D) expression in proliferative and secretory mouse uterus samples. Uterine tissue sections were incubated with rabbit antibodies against L-PGDS (C) and H-PGDSs (D) (in red), and nuclei were stained with the Hoescht dye (HST, in blue). (**E-F**) Representative immunofluorescence panels of DP1 (E) and DP2 (F) expression (in red) in proliferative mouse uterus samples. Nuclei were stained with the Hoescht dye (HST, in blue). iml: inner myometrium layer; JZ: junctional zone; ES: endometrial stroma; GE: glandular epithelium and LE: luminal epithelium. Dashed lines

delineate the JZ between ES and iml, and areas in the dashed squares are enlarged on the right panels. Scale bars: 150 μm (C-F).

Figure 2 Prostaglandin pathways are modified in *L/H-Pgds*$^{-/-}$ uteri. (**A-B**) Real-time quantitative RT-PCR analysis of genes encoding factors involved in prostaglandin synthesis in proliferative (A) and secretory (B) wild type (WT, in black) and *L/H-Pgds*$^{-/-}$ (KO, in grey) uteri. Data were normalised to *18S* expression. (A-B) Relative qPCR expression values are the mean +/- SEMs of 5 samples/genotype. P-values: *P<0.05, **P<0.01, ***P<0.005, ****P<0.0001. (**C**) Quantification of COX-1 and COX-2 staining intensity in the endometrial stroma (ES) and luminal epithelium (LE) (n=3 to 4 regions of interest for each compartment) of proliferative WT and KO uterus samples. Staining intensities are the mean +/- SEMs of n=3-5 uterine samples/genotype. P-values: **P<0.01, ****P<0.0001. (**D-G**) Dosage by ELISA of PGE2 (D), PGF2α (E) PGI2 (F) and PGD2 (G) in proliferative and secretory WT and *L/H-Pgds*$^{-/-}$ (KO) uteri (n=4 to 7 for prostaglandin dosage). For PGD2 levels, data are represented as the sum of proliferative and secretory values for WT and KO uteri (G). Prostaglandin levels (mean ± SEMs) were normalised to tissue weight and expressed in pg/mg tissue.

Figure 3 **Steroidogenesis is modified in *L/H-Pgds*$^{-/-}$ uteri**. (**A**) Real time quantitative RT-PCR analysis of steroidogenic gene levels normalised to *18S* expression in proliferative wild type (WT, in black) and *L/H-Pgds*$^{-/-}$ (KO, in grey) uteri. (**B-C**) 17β-oestradiol (E2) (B) was quantified in proliferative control (WT) and *L/H-Pgds*$^{-/-}$ uteri (n=6/genotype) by ELISA and progesterone (C) was quantified in proliferative and secretory control (WT) and *L/H-Pgds*$^{-/-}$ (KO) uteri (n=4 to 7/genotype) by LC-MS/MS. Steroid levels were normalised to the tissue weight and expressed in pg/mg tissue and represent the mean ± SEMs. (**D**) Representative immunofluorescence images of CYP19a1 expression localisation in *L/H-Pgds*$^{+/+}$ and *L/H-Pgds*$^{-/-}$ uteri in the proliferative phase of the oestrous cycle. Areas in the dashed white squares are enlarged in the lower panels. ES: endometrial stroma; GE: glandular epithelium and LE: luminal epithelium. Scale bar= 150 μm. **(E)** Quantification of CYP19a1 staining intensity in the endometrial stroma (ES), and luminal epithelium (LE) (n=3 to 4 ROIs for each compartment) of proliferative WT and KO uterus samples. Staining intensities are the mean +/- SEMs of n=3-5 uterine samples/genotype. P-values: *P<0.05, **P<0.01. (**F**) Real time quantitative RT-PCR analysis of *Hsd17B* gene levels normalised to *18S* expression in proliferative wild type (WT, in black) and *L/H-Pgds*$^{-/-}$ (KO, in grey) uteri. (A, F) Relative qPCR expression values are the mean +/- SEMs of 5 samples/genotype. P-values: *P<0.05, **P<0.01, ***P<0.005, ****P<0.0001.

Figure 4 In *L/H-Pgds*$^{-/-}$ females, lack of PGD2 promotes adenomyosis. **(A-B)** Representative images of uterus samples from 6-month-old wild type *L/H-Pgds*$^{+/+}$ (A) and mutant *L/H-Pgds*$^{-/-}$ (B) females after haematoxylin-eosin staining. The area within the dashed purple squares in the upper panels (A1, B1-B3) is enlarged in the lower panels (A1', B1'-B3') to visualise the endometrium/myometrium junction (JZ, dashed black line) and to highlight adenomyotic lesions (black arrows) in *L/H-Pgds*$^{-/-}$ uteri (B); Representative lesions are shown, Grade 1 (slight adenomyosis) (B1-B1'); Grade2 (moderate adenomyosis) (B2-B2') and Grade 3 (severe adenomyosis) (B3-B3'). (**C**) Histogram showing adenomyosis frequency in *L/H-Pgds*$^{+/+}$ (WT) and *L/H-Pgds*$^{-/-}$ (KO) females at the indicated ages (m: months). Adenomyosis frequency was expressed as the percentage of animals without adenomyosis (Grade 0), Grade 1, Grade 2 and Grade 3 lesions relative to all analysed mice. (**D-E**) Representative images of uterus samples from 12-month-old *L/H-Pgds*$^{+/+}$ (D) and *L/H-Pgds*$^{-/-}$ (E) females after haematoxylin-eosin staining. The dashed black line delineates the JZ at the endometrium/myometrium junction (D) and the area within dashed purple squares (D1, E1-E2) is enlarged in the lower panels (D1', E1'-E2') to show adenomyotic lesions (black arrows). (A-B, D-E) oml: outer myometrium layer; iml: inner myometrium layer; JZ: junctional zone; ES: endometrial stroma;

GE: glandular epithelium and LE: luminal epithelium. Scale bars: 300μm (A-B 1-3, D-E 1-2) and 150μm (A1', B1'-B3', D1', E1'-E2').

Figure 5 Characterisation of the *L/H-Pgds*$^{-/-}$ uterus phenotype. (**A-B**) Representative immunohistochemistry images of pan-cytokeratin (A) and α–Sma (B) expression in serial sections in the uterus of 6-month-old *L/H-Pgds*$^{+/+}$ and *L/H-Pgds*$^{-/-}$ females at the proliferative stage of the oestrous cycle and in an adenomyotic uterus (*L/H-Pgds-/-* Adm); (**C**) Representative images of picro-sirius red staining highlighting collagen fibres in uteri from *L/H-Pgds*$^{+/+}$ and *L/H-Pgds*$^{-/-}$ females and in an adenomyotic uterus (*L/H-Pgds*$^{-/-}$ Adm) at the proliferative stage of the oestrous cycle. Black arrows (A-C) indicate adenomyotic lesions in *L/H-Pgds*$^{-/-}$ uteri. (A-C) Oml: outer myometrium layer; iml: inner myometrium layer; JZ: junctional zone; ES: endometrial stroma; GE: glandular epithelium; LE: luminal epithelium. Scale bars: 300μm (A-C).

Figure 6 Adenomyosis biomarker identification in *L/H-Pgds*$^{-/-}$ uteri. Representative immunostaining images of Ki67 (**A**) and CD31 (**C**) expression in 6-month-old *L/H-Pgds*$^{+/+}$ and *L/H-Pgds*$^{-/-}$ uteri, and in adenomyotic lesions (*L/H-Pgds*$^{-/-}$ Adm). Dashed black lines delineate the junctional zone (JZ) between endometrial stroma and myometrium. Black arrows highlight

proliferating cells (A) and blood micro-vessels (B); black arrowheads identify adenomyotic lesions. Scale bar= 150 μm. (**B, D**) Quantification of Ki67 (B) and CD31 (D) staining density in the endometrial stroma (ES)-junctional zone (JZ) and inner myometrium (iml) of *L/H-Pgds*$^{+/+}$ (WT) and *L/H-Pgds*$^{-/-}$ (KO) uteri. Data are shown as the mean +/- SEMs (n=3 to 6 ROIs overlapping the ES-JZ-iml zones) of WT and KO uteri (n= 5/genotype). P-values: ****P<0.0001. (**E**) Representative immunofluorescence images of vimentin expression (in red) in 6-month-old *L/H-Pgds*$^{+/+}$ and *L/H-Pgds*$^{-/-}$ uteri, and adenomyotic lesions (*L/H-Pgds*$^{-/-}$ Adm); nuclei were stained with Hoescht (HST, in blue). Dashed white lines delineate the endometrial stroma/myometrium junction. White arrow identifies an adenomyotic lesion. Oml: outer myometrium layer; iml: inner myometrium layer; ES: endometrial stroma; GE: glandular epithelium and LE: luminal epithelium. Scale bars: 300μm (A-C).

Figure 7 **Model of adenomyotic lesion formation in the absence of PGD2 signalling**. In the non-pregnant uterus, PGDS synthases produce PGD2, in the endometrial stroma, junctional zone and myometrium. In *L/H-Pgds*$^{-/-}$ uteri, in the absence of PGD2 signalling, PGE2 secretion is increased and COX-2 protein expression is up-regulated. Similarly, the *StAR* gene, which encodes the rate-limiting factor in steroid biosynthesis, is up-regulated. Moreover, the expression of 17*Hsdbs* genes, which encode E2 metabolic enzymes is modified, the protein

level of CYP19a1 is increased and the subcellular localisation of ERα, ERβ are modified, in the endometrial stroma. These modified prostaglandin pathways and steroidogenesis lead to the induction of endometrial and myometrial cell proliferation, angiogenesis, and overexpression of vimentin and α–SMA and collagen deposition in the endometrial stroma, inducing epithelial-mesenchymal transition (EMT) and fibroblast-mesenchymal transition (FMT) in the endometrial stroma and endometrial-myometrium junctional zone. These features, induced directly or indirectly by the lack of PGD2, may contribute to inflammatory stimulation, uterine hyperperistalsis and injury, thus increasing the susceptibility to endometrial gland invagination and adenomyosis formation in the myometrium of *L/H-Pgds*$^{-/-}$ uteri.

Supplementary Figure S1 Representative immunofluorescence images of PGES-1 (**A**, in red), COX-1 (**B**, in green), COX-2 (**C**, in red), ERα (**D**, in green) and ERβ (**E**, in green) localisation in *L/H-Pgds*$^{+/+}$ and *L/H-Pgds*$^{-/-}$ uteri at the proliferative stage of the oestrous cycle. Nuclei were stained with Hoescht (HST, in blue). iml: inner myometrium layer; JZ: junctional zone; ES: endometrial stroma; GE: glandular epithelium and LE: luminal epithelium. Scale bar= 100 μm.

896

897

898

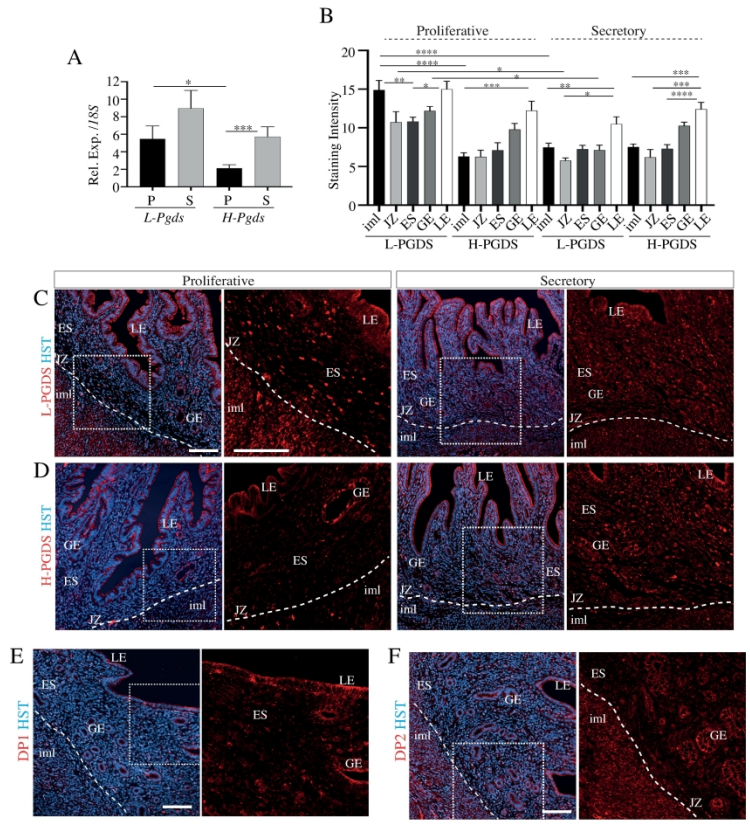

Figure 1

Figure 1 Expression of prostaglandin D2 synthases in wild type mouse uterus. (A) L-Pgds and H-Pgds gene expression were analysed by real time quantitative RT-PCR in mouse uteri collected at proliferative (P) and secretory (S) phases of the oestrous cycle. Results were normalised to 18S mRNA level and were compared with the Student's t test; *P<0.05, ***P<0.005. (B) Quantification of L-PGDS and H-PGDS staining intensity in the inner myometrium layer (iml), junctional zone (JZ), endometrial stroma (ES), glandular epithelium (GE) and luminal epithelium (LE) (n=3 to 4 ROIs for each compartment) of proliferative and secretory mouse uterus samples. Staining intensities are the mean +/- SEMs for n=3-5 uterine samples/phase. P-values: *P<0.05, **P<0.01, ***P<0.005, ****P<0.0001. (C-D) Representative immunofluorescence panels of L-PGDS (C) and H-PGDS (D) expression in proliferative and secretory mouse uterus samples. Uterine tissue sections were incubated with rabbit antibodies against L-PGDS (C) and H-PGDSs (D) (in red), and nuclei were stained with the Hoescht dye (HST, in blue). (E-F) Representative immunofluorescence panels of DP1 (E) and DP2 (F) expression (in red) in proliferative mouse uterus samples. Nuclei were stained with the Hoescht dye (HST, in blue). iml: inner myometrium layer; JZ: junctional zone; ES: endometrial stroma; GE: glandular epithelium and LE: luminal epithelium. Dashed lines delineate the JZ between ES and iml, and

areas in the dashed squares are enlarged on the right panels. Scale bars: 150 □m (C-F).

252x304mm (600 x 600 DPI)

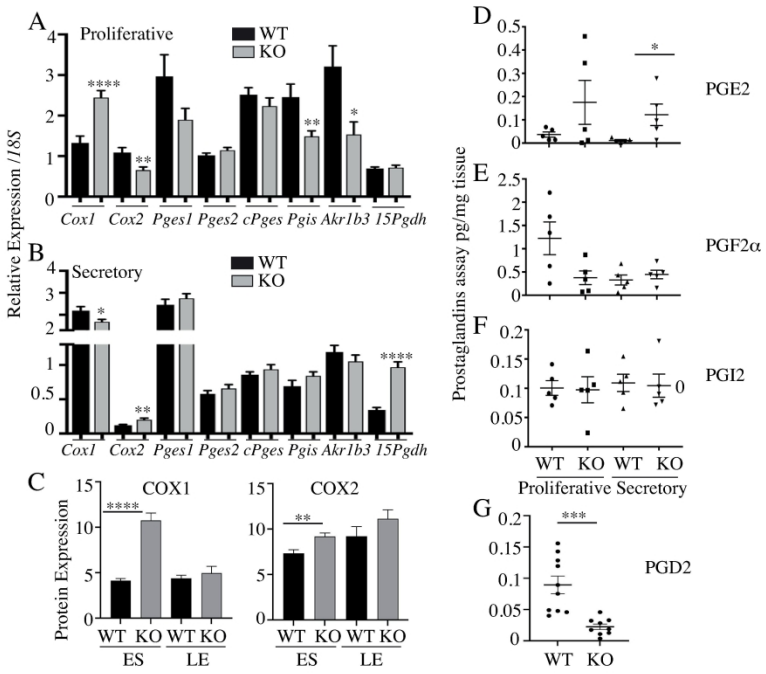

Figure 2

Figure 2 Prostaglandin pathways are modified in L/H-Pgds-/- uteri. (A-B) Real-time quantitative RT-PCR analysis of genes encoding factors involved in prostaglandin synthesis in proliferative (A) and secretory (B) wild type (WT, in black) and L/H-Pgds-/- (KO, in grey) uteri. Data were normalised to 18S expression. (A-B) Relative qPCR expression values are the mean +/- SEMs of 5 samples/genotype. P-values: *P<0.05, **P<0.01, ***P<0.005, ****P<0.0001. (C) Quantification of COX-1 and COX-2 staining intensity in the endometrial stroma (ES) and luminal epithelium (LE) (n=3 to 4 ROIs for each compartment) of proliferative WT and KO uterus samples. Staining intensities are the mean +/- SEMs of n=3-5 uterine samples/genotype. P-values: **P<0.01, ****P<0.0001. (D-G) Dosage by ELISA of PGE2 (D), PGF2□ (E) PGI2 (F) and PGD2 (G) in proliferative and secretory WT and L/H-Pgds-/- (KO) uteri (n=4 to 7 for prostaglandin dosage). For PGD2 levels, data are represented as the sum of proliferative and secretory values for WT and KO uteri (G). Prostaglandin levels (mean ± SEMs) were normalised to tissue weight and expressed in pg/mg tissue.

170x226mm (600 x 600 DPI)

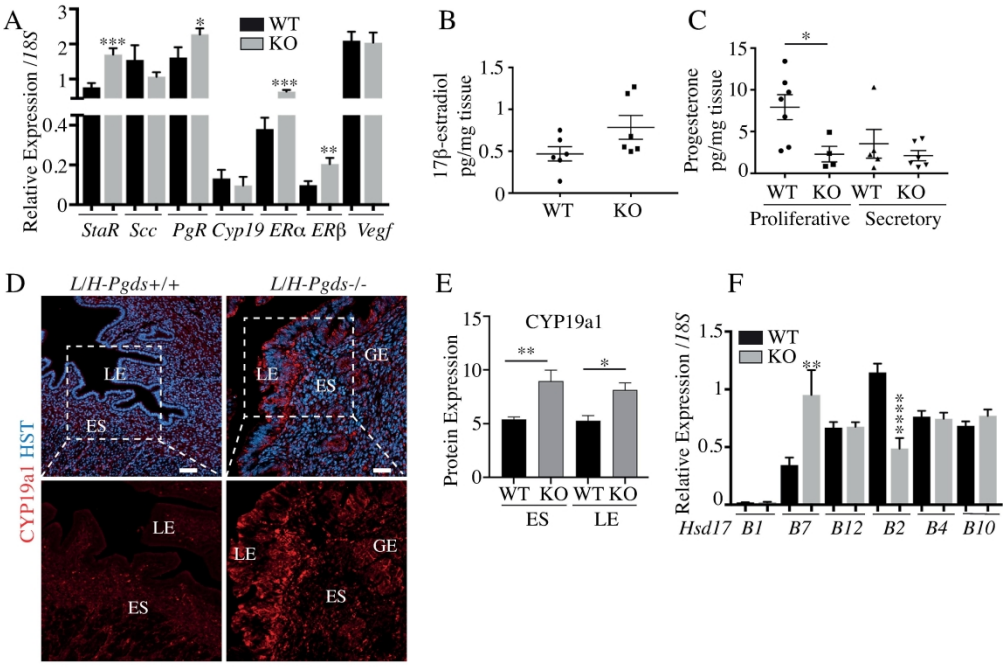

Figure 3

Figure 3 Steroidogenesis is modified in L/H-Pgds-/- uteri. (A) Real time quantitative RT-PCR analysis of steroidogenic gene levels normalised to 18S expression in proliferative wild type (WT, in black) and L/H-Pgds-/- (KO, in grey) uteri. (B-C) 17□-oestradiol (E2) (B) was quantified in proliferative control (WT) and L/H-Pgds-/- uteri (n=6/genotype) by ELISA and progesterone (C) was quantified in proliferative and secretory control (WT) and L/H-Pgds-/- (KO) uteri (n=4 to 7/genotype) by LC-MS/MS. Steroid levels were normalised to the tissue weight and expressed in pg/mg tissue, and represent the mean ± SEMs. (D) Representative immunofluorescence images of CYP19a1 expression localisation in L/H-Pgds+/+ and L/H-Pgds-/- uteri in the proliferative phase of the oestrous cycle. Areas in the dashed white squares are enlarged in the lower panels. ES: endometrial stroma; GE: glandular epithelium and LE: luminal epithelium. Scale bar= 150 □m. (E) Quantification of CYP19a1 staining intensity in the endometrial stroma (ES), and luminal epithelium (LE) (n=3 to 4 ROIs for each compartment) of proliferative WT and KO uterus samples. Staining intensities are the mean +/- SEMs of n=3-5 uterine samples/genotype. P-values: *P<0.05, **P<0.01. (F) Real time quantitative RT-PCR analysis of Hsd17B gene levels normalised to 18S expression in proliferative wild type (WT, in black) and L/H-Pgds-/- (KO, in grey) uteri. (A, F) Relative qPCR expression values are the mean +/- SEMs of 5 samples/genotype. P-values: *P<0.05, **P<0.01, ***P<0.005, ****P<0.0001.

176x146mm (600 x 600 DPI)

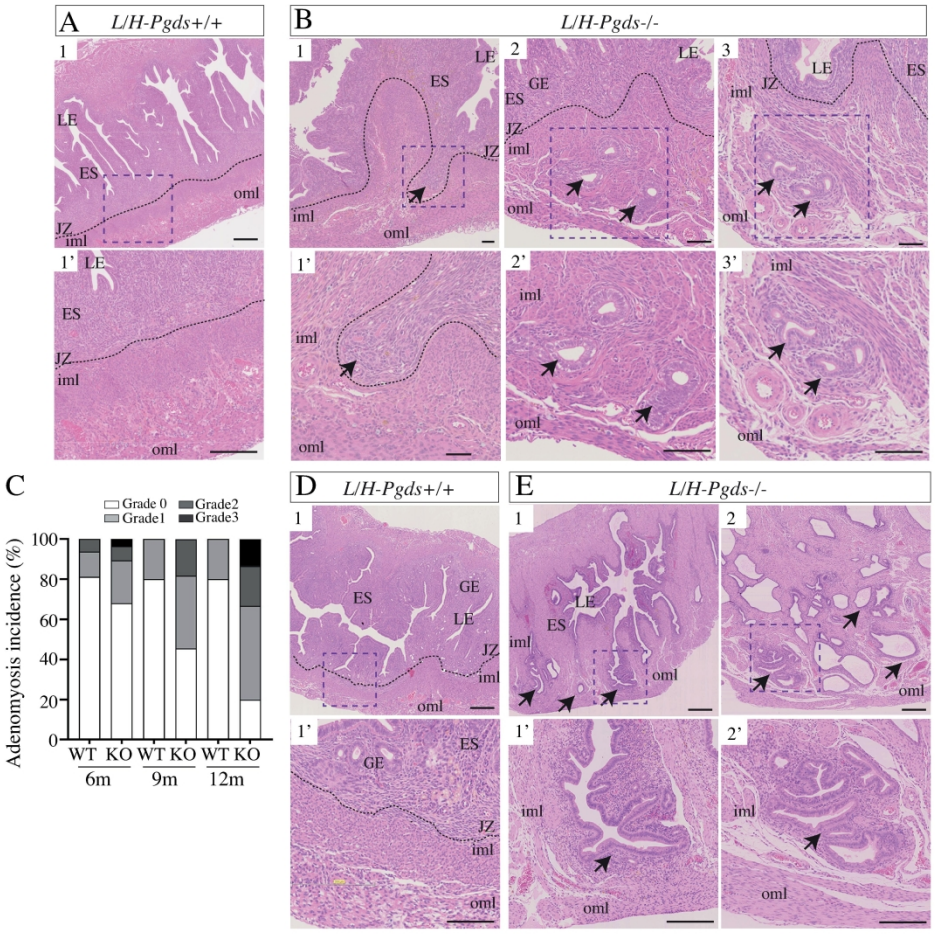

Figure 4

Figure 4 In L/H-Pgds-/- females, lack of PGD2 promotes adenomyosis. (A-B) Representative images of uterus samples from 6-month-old wild type L/H-Pgds+/+ (A) and mutant L/H-Pgds-/- (B) females after haematoxylin-eosin staining. The area within the dashed purple squares in the upper panels (A1, B1-B3) is enlarged in the lower panels (A1', B1'-B3') to visualise the endometrium/myometrium junction (JZ, dashed black line) and to highlight adenomyotic lesions (black arrows) in L/H-Pgds-/- uteri (B); Representative lesions are shown, Grade 1 (slight adenomyosis) (B1-B1'); Grade2 (moderate adenomyosis) (B2-B2') and Grade 3 (severe adenomyosis) (B3-B3'). (C) Histogram showing adenomyosis frequency in L/H-Pgds+/+ (WT) and L/H-Pgds-/- (KO) females at the indicated ages (m: months). Adenomyosis frequency was expressed as the percentage of animals without adenomyosis (Grade 0), Grade 1, Grade 2 and Grade 3 lesions relative to all analysed mice. (D-E) Representative images of uterus samples from 12-month-old L/H-Pgds+/+ (D) and L/H-Pgds-/- (E) females after haematoxylin-eosin staining. The dashed black line delineates the JZ at the endometrium/myometrium junction (D) and the area within dashed purple squares (D1, E1-E2) is enlarged in the lower panels (D1', E1'-E2') to show adenomyotic lesions (black arrows). (A-B, D-E) oml: outer myometrium layer; iml: inner myometrium layer; JZ: junctional zone; ES: endometrial stroma; GE: glandular epithelium and LE: luminal epithelium. Scale bars: 300□m (A-B 1-3, D-E 1-2) and 150□m (A1', B1'-B3', D1', E1'-E2').

190x203mm (600 x 600 DPI)

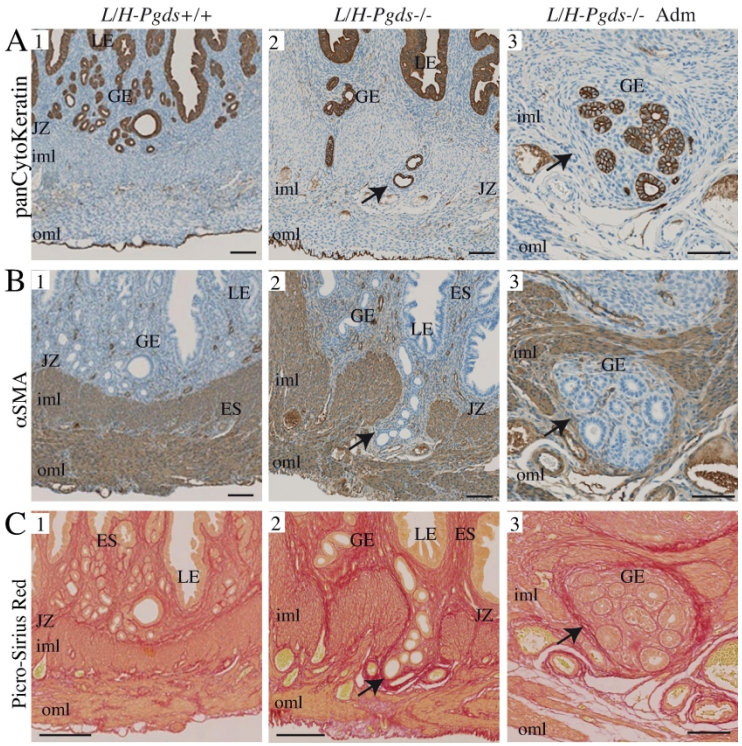

Figure 5

Figure 5 Characterisation of the L/H-Pgds-/- uterus phenotype. (A-B) Representative immunohistochemistry images of pan-cytokeratin (A) and □□Sma (B) expression in serial sections in the uterus of 6-month-old L/H-Pgds+/+ and L/H-Pgds-/- females at the proliferative stage of the oestrous cycle and in an adenomyotic uterus (L/H-Pgds-/- Adm); (C) Representative images of picro-sirius red staining highlighting collagen fibres in uteri from L/H-Pgds+/+ and L/H-Pgds-/- females and in an adenomyotic uterus (L/H-Pgds-/- Adm) at the proliferative stage of the oestrous cycle. Black arrows (A-C) indicate adenomyotic lesions in L/H-Pgds-/- uteri. (A-C) Oml: outer myometrium layer; iml: inner myometrium layer; JZ: junctional zone; ES: endometrial stroma; GE: glandular epithelium; LE: luminal epithelium. Scale bars: 300□m (A-C).

173x145mm (600 x 600 DPI)

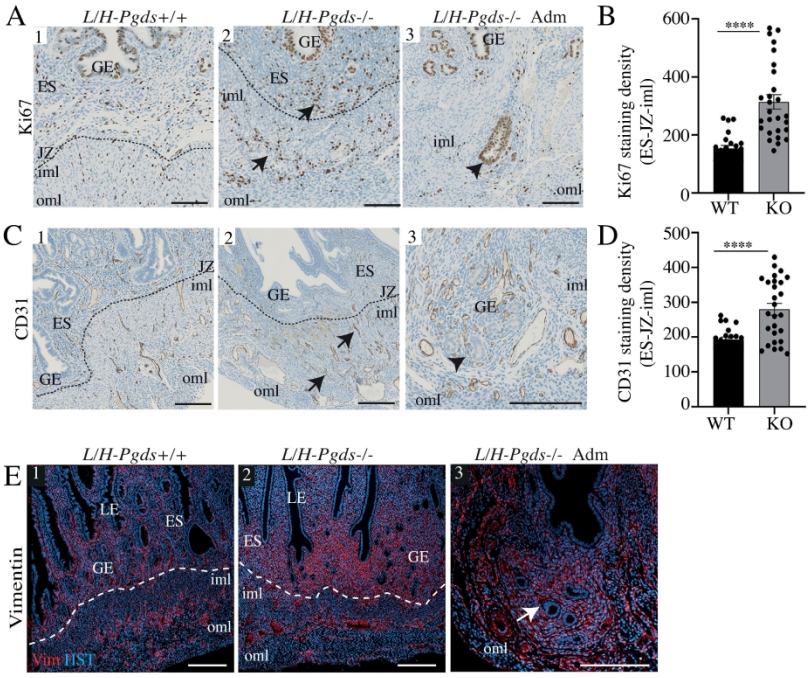

Figure 6

Figure 6 Adenomyosis biomarker identification in L/H-Pgds-/- uteri. Representative immunostaining images of Ki67 (A) and CD31 (C) expression in 6-month-old L/H-Pgds+/+ and L/H-Pgds-/- uteri, and in adenomyotic lesions (L/H-Pgds-/- Adm). Dashed black lines delineate the junctional zone (JZ) between endometrial stroma and myometrium. Black arrows highlight proliferating cells (A) and blood micro-vessels (B); black arrowheads identify adenomyotic lesions. Scale bar= 150 □m. (B, D) Quantification of Ki67 (B) and CD31 (D) staining density in the endometrial stroma (ES)-junctional zone (JZ) and inner myometrium (iml) of L/H-Pgds+/+ (WT) and L/H-Pgds-/- (KO) uteri. Data are shown as the mean +/- SEMs (n=3 to 6 ROIs overlapping the ES-JZ-iml zones) of WT and KO uteri (n= 5/genotype). P-values: ****P<0.0001. (E) Representative immunofluorescence images of vimentin expression (in red) in 6-month-old L/H-Pgds+/+ and L/H-Pgds-/- uteri, and adenomyotic lesions (L/H-Pgds-/- Adm); nuclei were stained with Hoescht (HST, in blue). Dashed white lines delineate the endometrial stroma/myometrium junction. White arrow identifies an adenomyotic lesion. Oml: outer myometrium layer; iml: inner myometrium layer; ES: endometrial stroma; GE: glandular epithelium and LE: luminal epithelium. Scale bars: 300□m (A-C).

158x231mm (600 x 600 DPI)

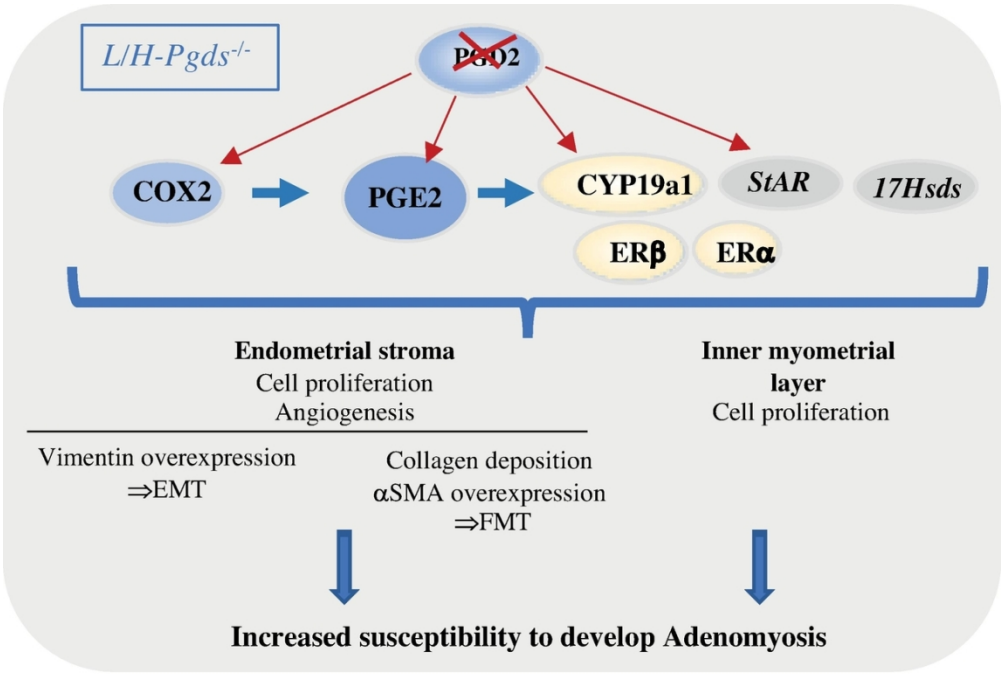

Figure 7

109x92mm (300 x 300 DPI)